Egypt. J. Chem. **Vol.** 68, SI: Z. M. Nofal, pp. 1009- 1031(2025)

Egyptian Journal of Chemistry

http://ejchem.journals.ekb.eg/

Eco-friendly High-Density Polyethylene Nanocomposites Reinforced with Rice Straw-Derived Nanocellulose: Synthesis, Characterization, and Biodegradability Assessment

Ghada A. Kadry[a*], Heba A. El- Gawad[b], Mostafa H. Hussein[a]

[a] *Chemical Engineering Department, The Higher Institute of Engineering, El Shorouk Academy, Cairo Egypt*
[b] *Engineering Mathematics and Physics Department, The Higher Institute of Engineering, El Shorouk Academy, Cairo, Egypt*

Abstract

This study presents an innovative strategy for fabricating sustainable nanocomposites by using rice straw, a common agricultural byproduct, as a reinforcing agent for high-density polyethylene (HDPE). This research integrates waste valorisation, nanomaterial synthesis, and polymer engineering to develop materials with enhanced properties and a reduced environmental impact. The mechanical, thermal, and biodegradation characteristics of the resulting composites were thoroughly investigated. Nanocellulose, extracted from rice straw through a series of treatments (alkaline pulping, bleaching, and acid hydrolysis), resulted in particles with diameters between 15 and 24 nm. Composites with nanocellulose loadings between 0.1% and 7% demonstrated notable improvements in mechanical performance. The tensile strength increased by as much as 14.38%, and the elastic modulus showed an enhancement of up to 31.50% at an optimal nanocellulose loading range of 0.4% to 0.8%. Spectroscopic analysis confirmed enhanced thermal stability and evidence of interaction between HDPE and nanocellulose. Furthermore, preliminary biodegradation tests indicated a partial degradation of 0.28% over five months through soil burial tests, showing that nanocellulose incorporation facilitates environmental decomposition

Keywords: Nanocellulose; HDPE nanocomposites; Sustainable materials; Biodegradability; Thermal stability; Mechanical properties; Eco-friendly composites.

1. Introduction

The increasing global focus on environmental sustainability has driven a surge in research and development of eco-friendly materials [1]. Among these, nanocomposites reinforced with cellulose nanofibers (CNF) have emerged as promising candidates due to their superior mechanical properties compared to traditional micro-composites [2].

Nanoelements can be derived from various renewable sources, including cellulose, starch, and chitin [3]. However, cellulose, being the most abundant polymer, has been the primary focus of research. Cellulosic materials are often used as fillers in biocomposites, though they frequently enhance rigidity at the expense of ductility. These nanoparticles, often referred to as whiskers or nanocrystals, are elongated crystalline structures obtained through the removal of amorphous cellulose regions, typically via acid hydrolysis [4].

Cellulose, the most abundant natural polymer, is derived from various plant sources and possesses unique characteristics that make it a desirable material for biodegradable and renewable applications [5, 6].

Concurrently, the disposal of agricultural waste, such as rice straw, often results in practices like open-field burning, contributing to air pollution [7–9]. Addressing these dual environmental concerns requires innovative approaches that can transform waste materials into value-added products while enhancing the properties of commonly used polymers [9–13].

Nanocellulose, derived from plant-based sources, has emerged as a promising material for reinforcing polymer composites due to its high strength, large surface area, and potential to improve material properties. The valorisation of crop residues is increasingly important, especially with the growing biofuel industry. The extraction of nanocellulose from agricultural waste offers a dual benefit: valorising waste and creating high-performance composite materials. Rice straw, an abundant agricultural byproduct, represents an ideal source for nanocellulose extraction, offering a sustainable alternative to conventional reinforcing agents [8, 14]. Traditionally used in paper and composite panels, particularly in regions with limited wood resources [13].

*Corresponding author e-mail: g.kadry@sha.edu.eg, Kadryghada@yahoo.com; (Ghada Ahmed Kadry).
Received date 06 August 2025; Revised date 12 September 2025; Accepted date 21 September 2025
DOI: 10.21608/ejchem.2025.411431.12147

The production of nanocellulose-reinforced composites traditionally involves two separate steps: nano-fibrillation of cellulose and subsequent incorporation into polymer matrices. These processes can be energy-intensive, time-consuming, and costly [2]. Recent research has focused on developing more efficient, one-step methods for simultaneous nano-fibrillation and nanocomposite production, aiming to overcome these limitations.

Various techniques have been explored for cellulose nano-fibrillation, including chemical treatments, mechanical processes, and enzymatic approaches [14, 15]. Each method presents its own set of advantages and challenges, particularly concerning environmental impact and scalability. Similarly, different strategies have been investigated to improve the compatibility between hydrophilic cellulose nanofibers and hydrophobic polymer matrices like HDPE, ranging from chemical modifications to the use of compatibilizing agents [1, 18–20].

Understanding the thermal behaviour of cellulose-based composites is crucial for optimizing their processing and performance [21, 22]. The high crystallinity of cellulose and its tendency to form hydrogen bonds present unique challenges in composite manufacturing, necessitating careful consideration of processing conditions [23, 24].

The widespread use of synthetic polymers, particularly high-density polyethylene (HDPE), has led to significant environmental challenges due to their persistence and resistance to degradation [21, 25]. High-density polyethylene (HDPE) is a versatile, semi-crystalline thermoplastic polymer widely used in various industries and consumer products [26], especially in food packaging, presents environmental challenges due to its persistence and resistance to degradation. Incorporating cellulose nanofibers into HDPE has the potential to enhance the material's biodegradability while maintaining or improving its functional properties [21].

This study presents an integrated approach to sustainable material development by using rice straw, an agricultural waste, to reinforce a high-density polyethylene (HDPE) matrix. By focusing on the production of nanocellulose from rice straw, followed by a detailed assessment of the resulting composites, the research combines principles of waste valorisation, nanomaterial engineering, and polymer science to synthesize a material with enhanced performance and a reduced environmental footprint. The final composites are evaluated for their mechanical, thermal, and biodegradation properties, demonstrating a pathway to synthesize high-performance materials while also introducing biodegradable elements into a standard non-biodegradable polymer.

This research makes several significant contributions to the field of sustainable materials. First, it offers a comprehensive approach to valorising agricultural waste by extracting and characterizing nanocellulose from rice straw. Second, it demonstrates the effective use of this bio-derived nanomaterial as a reinforcing agent in a high-density polyethylene (HDPE) matrix. Finally, the study provides a detailed analysis of the mechanical, thermal, and biodegradation properties of the resulting nanocomposites, offering a complete picture of the material's enhanced performance and environmental benefits.

The study stands out by offering a practical solution that bridges waste management, materials science, and environmental sustainability. By finding an effective way to reinforce plastics with agricultural waste-derived nanoparticles, the research presents a promising pathway for developing more eco-friendly materials with enhanced structural characteristics. This approach not only addresses the global challenge of waste management but also opens new possibilities for creating high-performance, sustainable materials that can potentially replace traditional petroleum-based composites.

2. Experimental work

2.1 Materials

Rice straw, sourced from local Egyptian farmers in "Shebin- El Kanater – Qaluobia", served as the biomass raw material for the natural lignocellulosic fiber. The straw was dried to a moisture content of 7-9% at room temperature. Sodium hypochlorite (≥ 5% w/v), sodium hydroxide, chlorine, sodium chlorite, acetic acid, and sulfuric acid (72% w/w) were obtained from El Nasr Company for Chemicals. A powder form of high-density polyethylene (HDPE) was sourced from SABIC (grade CC860V), with assistance from the National Research Center. The material's technical specifications indicate a density of 0.96 g/cm³ and a molecular weight of 78,000 g/mol.

2.1 Methodology

2.2.1. Rice straw composition

The physicochemical properties of rice straw, including moisture content, ash content, volatile organic matter, fixed carbon yield, α-cellulose, hemicellulose, and lignin content, were determined using established analytical methods.

i. Moisture content

Moisture content was determined using the ASTM D2867-91 method [27]. A crucible containing 3 grams of rice straw was weighed, placed in an electric hot air oven at 110°C for 2 hours, cooled in a desiccator, and reweighed. This process was repeated until a constant weight was achieved. Moisture content was calculated as a percentage using Equation (1) [28, 29]:

$$\textbf{Moisture content} = \frac{(W1+W2)-W3}{W2} * 100 \qquad (1)$$

Where: W_1 represents the weight of the empty crucible, W_2 is the weight of rice straw, and W_3 is the weight of residue after drying at 110°C.

ii. Ash content

The ash content in rice straw was determined using an ignition method. Rice straw was cut into small pieces, and a weighed sample (approximately 1gram) was placed in a porcelain crucible and heated in a muffle furnace at 400°C for 30 minutes, followed by 850°C for 45 minutes. The remaining ash was then weighed, and the ash percentage was calculated using equation (2) [30–32].

$$\boldsymbol{Ash}\% = \frac{\boldsymbol{weight\ of\ ash,\ g}}{\boldsymbol{weight\ of\ dry\ sample,\ g}} x100 \quad \textbf{(2)}$$

iii. Volatile matter

Approximately 1.5grams of dried rice straw was placed in a pre-weighed crucible. Following the method described by Heavner et al. (1996) [33], the crucible was heated in a muffle furnace at 925°C for 90 minutes. After cooling in a desiccator, the crucible was weighed again. The volatile organic matter content was calculated using Equation (3) [28].

$$\text{Volatile matter}\% = \frac{\boldsymbol{Weight\ of\ volatile\ components,\ g}}{\boldsymbol{Oven\ dried\ weight,\ g}} * 100 \quad \textbf{(3)}$$

iv. Fixed carbon yield

The total carbon yield was determined using the loss-on-ignition method. The fixed carbon yield was calculated using equation (4) [28].

$$\text{Carbon yield} = \frac{\boldsymbol{weight\ of\ carbon\ retrieved\ from\ furnace,g}}{\boldsymbol{dried\ weight\ of\ carbon\ sample,g}} = 100 \quad \textbf{(4)}$$

v. α -Cellulose and Hemicellulose content

To determine α-cellulose content, holocellulose must be initially estimated. Holocellulose was prepared using a sodium chlorite ($NaClO_2$) method. Approximately 5grams of extracted rice straw was added to 80 mL of distilled water at 75°C and stirred mechanically. Acetic acid (0.8mL) and sodium chlorite (1.86grams) were then added, and the mixture was stirred vigorously until the lignin colour faded. The remaining holocellulose was washed with distilled water, acetone, and ether before being dried under vacuum at 50°C. Holocellulose (approximately 3 grams) was treated with 25mL of 17.5% (w/w) sodium hydroxide and allowed to swell for 4 minutes at 20°C. The sample was pressed for 3 minutes with a glass rod, followed by the addition of another 25mL of NaOH and mixing for 1 minute. After 35 minutes, 100 mL of distilled water was added, and the mixture was filtered through a sintered glass funnel. 100mL of 10% acetic acid was added dropwise for washing, followed by distilled water. The α-cellulose percentage was determined gravimetrically after drying in a drying oven at 105°C and subtracting the ash content (Equation 2) [30–32].

$$\boldsymbol{\alpha - cellulose}\% = \frac{\boldsymbol{weight\ of\ \alpha-cellulose-weight\ of\ its\ ash}}{\boldsymbol{weight\ of\ original\ hollocellulose\ sample}} x100 \quad \textbf{(5)}$$

$$hemi - cellulose\% = holocellulose\% - \alpha - cellulose$$

vi. Lignin content

Lignin content in the raw material was estimated using a sulfuric acid method. Approximately one gram of accurately weighed material was treated with 72% sulfuric acid (w/w) at a liquor-to-solid ratio of 20:1 for 4 hours at room temperature (25-30°C). The mixture was then diluted to 3% sulfuric acid and boiled for 4 hours under reflux. The lignin was filtered using an ash-free filter paper and washed with hot distilled water until neutral. The lignin content was determined gravimetrically after ignition at 400°C for 30 minutes and 800°C for 45 minutes. The weight of the ash was subtracted to obtain the lignin-free ash, using Equation (3.3) [30–32, 34].

$$\boldsymbol{Lignin}\% = \frac{\boldsymbol{weight\ of\ lignin-weight\ of\ its\ ash}}{\boldsymbol{weight\ of\ the\ dry\ sample}} x\ 100 \quad \textbf{(6)}$$

In addition, FTIR spectra, zeta potential, and electronic structure of the rice straw were analysed using an FTS-40, USA FTIR spectroscopy using KBr discs with absorption mode in the range 4000– 400cm^{-1} with an accumulation of 32 scans and a resolution of 2cm^{-1}, an SZ-100 nanoparticle size and zeta potential analyser and a transmission electron microscope (TEM) (a JEOL model 1200EXelectron microscope running on an accelerating voltage at 120Ky), respectively. Scanning electron microscopy (SEM) was used to examine the surface morphology of the rice straw.

2.2.2. Chemical pulping process of rice straw

2.2.2.1. Alkaline pulping

Rice straw was cut into small pieces and added to a pressurized autoclave containing a 5% w/v sodium hydroxide solution with a liquor-to-solid ratio of 10:1.The mixture was heated to 160°C and pressurized to 15atm for 2 hours to separate cellulose fibers from the black liquor (lignin and hemicellulose) [8, 35]. The cellulose fibers were subsequently washed with warm water and bleached for further processing. For cardboard production, the bleached fibers could be directly used in the papermaking process.

2.2.2.1. Formic acid pulping

An investigation into the pulping of rice straw using formic acid explored various temperatures, cooking times, and acid concentrations. Under relatively mild conditions (100°C, 60 minutes, 90% formic acid), a delignification rate of approximately 85% with a pulp yield of 44.4% was achieved. The resulting pulp's chemical and mechanical properties were comparable to those obtained from pulping in alkaline environments. However, a significant advantage of formic acid pulping is the retention of most silicon derivatives within the pulp.

2.2.3. Bleaching process

The fibers obtained after the cooking process often exhibit a brownish colour due to residual lignin, which can adversely affect paper properties and whiteness. To achieve a high degree of brightness, the remaining lignin is removed through a bleaching process. Two common bleaching methods involve sodium hypochlorite (NaOCl > 5% w/v) and sodium chlorite ($NaClO_2$ > 5% w/v). The sodium chlorite bleaching process is typically conducted at atmospheric pressure and room temperature with a solid-to-liquor ratio of 1:10.

2.2.4. Synthesis of nanocellulose (NC)

Nanocellulose was extracted from rice straw pulp using sulfuric acid hydrolysis, following a method outlined in the literature [14]. The pulp was initially ground into fine particles using a Willey mill. A 10-gram sample of cellulose was then hydrolysed with 64% sulfuric acid for approximately 50 minutes at 50°C. Following this, the resulting mixture was washed with deionized water and neutralized to a pH of 6 via centrifugation and dialysis. The resulting dispersion was dried at 40°C.

Transmission electron microscopy (TEM) performed using a JEOL model 1200EX electron microscope operating at 120kV, was utilized to characterize the size of the nanocellulose particles, which fell within a specific range [8]. Fourier-transform infrared spectroscopy (FTIR) analysis was employed to investigate the structural changes in the rice straw, extracted cellulose, and nanocellulose. Zeta potential measurements were conducted using a Zetatrac instrument equipped with Microtrac FLEX Operating Software to assess the stability of the nanoparticles. Scanning electron microscopy (SEM) was employed to characterize nanocellulose surface morphology.

2.2.5. Preparation of nanocomposites

HDPE/nanocellulose nanocomposites were fabricated using a Brabender mixer. 180grams of HDPE was melt-mixed with varying nanocellulose loadings (0.1% to 7% by weight) at 180°C and 90 rpm for 8 minutes. The resulting mixtures were molded into 1-mm-thick sheets (15cm x 12cm) using a hot press at 170°C and 20MPa, followed by cooling.

The nanocomposites were subjected to various characterization techniques. FTIR spectroscopy was used to analyse chemical composition. Scanning electron microscopy (SEM) was employed to visualize nanocomposite surface morphology. TGA assessed thermal stability. Mechanical properties, including tensile strength, modulus, elongation, flexural strength, and impact strength, were evaluated according to ASTM standards. To assess biodegradability, the nanocomposites were buried in soil for four months. Weight loss measurements were taken weekly, with samples dried at 50°C to account for moisture absorption.

3. Results and discussion

3.1. Physicochemical characteristics of rice straw

Pulping and bleaching rice straw with formic acid resulted in lower ash and lignin content, as well as a brighter white colour of the cellulose compared to sodium hydroxide (Figure 1 and Table 1). This suggests that formic acid can be effectively used for pulping and bleaching processes at atmospheric pressure. However, it yielded a lower α-cellulose content in the treated samples. Consequently, due to a higher α-cellulose yield, sodium hydroxide was chosen and employed for the pulping and bleaching of rice straw, enabling the subsequent extraction of nanocellulose. Figure 1 and Table 1 present the physicochemical properties of rice straw.

Table 1: Physicochemical properties of rice straw

Material	Rice straw (raw material)	Pulping rice straw with NaOH	Pulping rice straw with Formic acid	Bleaching rice straw with NaOH	Bleaching rice straw with Formic
Yield %	100	70	59.14	64.76	50.26
ά-cellulose %	53.33	63.33	54.00	88.5	54.7
Hemi-cellulose %	5.46	3.8	2.71	0.953	2.786
Lignin %	30	20	8.7	4.2	4.16
Ash content %	4%	12.20%	8.33%	1.127%	0.564%
Moisture Content %	7.20%	5.40%	1.20%	7.00%	6.59%
Fixed carbon yield%	8.70%	6.70%	9.10%	8.00%	11.58%
Volatile matter %	56.90%	75.70%	76.50%	68.00%	52.39%

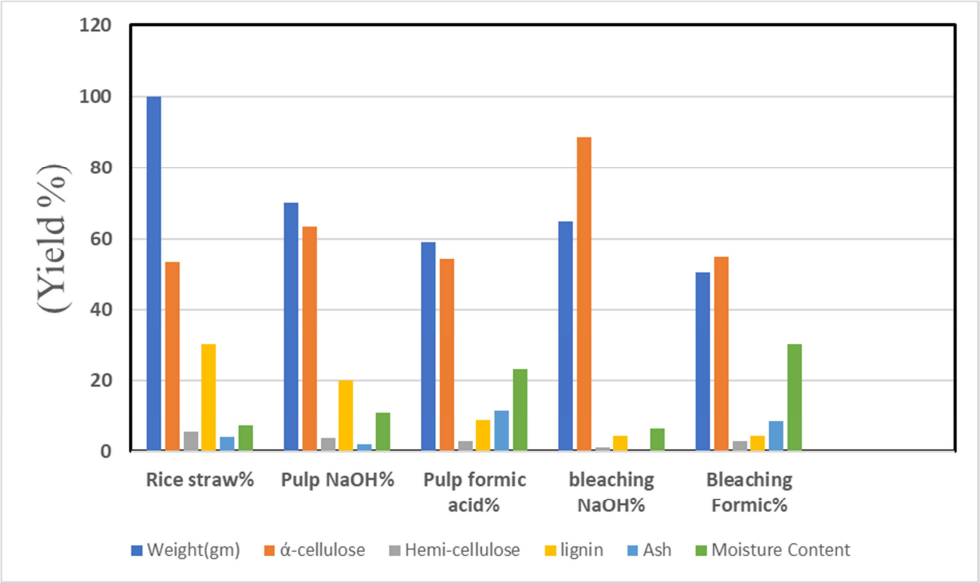

Figure 1: Physicochemical properties of rice straw

3.2. Characteristics of rice straw, cellulose, and Nanocellulose

i. Fourier transform infrared (FTIR) spectroscopy

The IR spectra of rice straw, commercial cellulose, extracted cellulose, and nanocellulose presented in Figure 2 and Table 2 revealed distinct peaks, enabling chemical characterization of the different samples [36–38]. The broad hydroxyl band at 3000-3500cm^{-1} in all samples indicates the presence of O-H groups in holocellulose (cellulose and hemicellulose). Additionally, peaks at 1158 and 1026cm^{-1} correspond to C-O-C stretching in cellulose and hemicellulose. The peaks at 2918cm^{-1} and 1370cm^{-1} represent C-H bonds in methyl and phenol groups of lignin and hemicellulose. The peak at 609cm^{-1} indicates the glycosidic β (1–4) linkage of cellulose. The 1735cm^{-1} peak corresponds to the C=O of the acetyl group from hemicellulose/lignin. The 1640cm^{-1} band represents aromatic skeleton stretching.

The extracted cellulose sample lacked peaks at 1740cm^{-1} and 1242cm^{-1}, associated with carbonyl and aromatic groups in lignin, suggesting efficient delignification during the pulping and bleaching treatment. However, a small shoulder was still present at 1740cm^{-1}, indicating some residual hemicellulose or lignin.

The spectra of extracted cellulose closely matched those of commercial cellulose [39], with distinct cellulose peaks visible at 671cm^{-1} (glycosidic bonds) and 1165cm^{-1} (secondary alcohols). This confirms the isolated product is predominantly cellulose with increased purity compared to the initial rice straw. In the nanocellulose, peaks at 1026 and 1158cm^{-1} corresponding to C-O-C stretch shifted to 1058 and 1165cm^{-1}, indicating the formation of inter- and intra-molecular hydrogen bonds during nano-fibrillation, which alter the cellulose structure. Crucially, the nanocellulose samples lacked peaks at

1735cm^{-1} and 1242cm^{-1} associated with carbonyl and aromatic groups in lignin [14, 40]. This suggests efficient delignification during the pulping and bleaching process and that the nanofibrillation process did not introduce new chemical groups.

FTIR analysis characterized the chemical structure and identified functional groups in cellulose extracted from rice straw using different pre-treatments. The broad peak at 3332cm^{-1} in all samples corresponded to O-H stretching vibrations of hydroxyl groups in the cellulose and hydrogen bonding. The peak at 2916cm^{-1} represented C-H stretching vibrations found in all polysaccharides. The absorption at 1211cm^{-1} was attributed specifically to C-O stretching vibrations in cellulose. Untreated rice straw showed peaks at 1640cm^{-1} and 1635cm^{-1} associated with aromatic C-C stretching in lignin, which were absent in all pre-treated cellulose samples, indicating effective lignin removal. The peak at 1438cm^{-1} related to C-H bending from lignin and polysaccharides was also missing in extracted cellulose. The cellulose-specific peak at 1026cm^{-1} corresponding to C-O-C pyranose ring vibrations was visible in all pre-treated samples.

FTIR analysis confirmed that the different pre-treatment methods (alkali, steam explosion, organogold) successfully removed non-cellulosic components, especially lignin, as evidenced by the disappearance of lignin-specific peaks while retaining peaks related to cellulose C-O and C-O-C vibrations. These results align with the compositional analysis and microscopy data, demonstrating effective isolation of cellulose from rice straw.

Table 2: FT-IR Spectra of: rice straw, extracted cellulose, commercial cellulose, and Nanocellulose.

		Rice straw [36]	**Commercial Cellulose** [39]	**Rice Straw**	**Extracted Cellulose**	**Nanocellulose**	**Appearance**
Molecules names	**Function groups**	**Wave number, cm^{-1}**					
Cellulose	O-H stretching intramolecular hydrogen bond	3500-3000	3391	3336	3332	3327	Increased
	C-H stretching of polysaccharide	2918	2906	2918	2916	2849	increased
	C- H_2 symmetric bending	1423	1423	1440	1418	1424	Increased
	C-H_2 bending	1430	1423	1440	1418	1424	Increased
	Cellulose C–H	1375	1373	-	1316	1308	Increased
	O-H stretching of secondary alcohol	1161	1162	-	1156	1153	Increased
	O-H stretching of primary alcohol	1026	1061	1025	1026	964	Increased
	O-H vibration of absorbed water [41]	-	-	1635	1644	1635	Increased
	C-O-C asymmetric stretching	1158	1155	-	1158	1162	Increased
	Glycosidic bond	600-850	609	791	661	660	Increased
Hemicellulose	C=O of acetyl or carboxylic acid	1735	1760	1740	1644	1635	Increased
	Glycosidic bond	600-850	608	791	661	660	Increased
	C-O-C	1026	1061	1025	1026	967	Increased
Lignin	C=O of acetyl or carboxylic acid	1690-1760	1760	1730	1644	1635	Disappear
	C-O stretching of phenols	1242	-	-	1211	1156	Disappear

	C=C stretching of the aromatic ring	1640	1635	1635	1644	1635	O-H vibration of absorbed water [57]
	C-H_3 Asymmetric bending or C-H angular deformation of methoxyl group in	1465 1457	1450	-	1438	1420	-
	Aromatic ring C-H	2840 – 3095	-	2918	2916	2849	Increased
	Phenolic compounds (PhOH.)	1370	1373	-	1323	1320	Increased

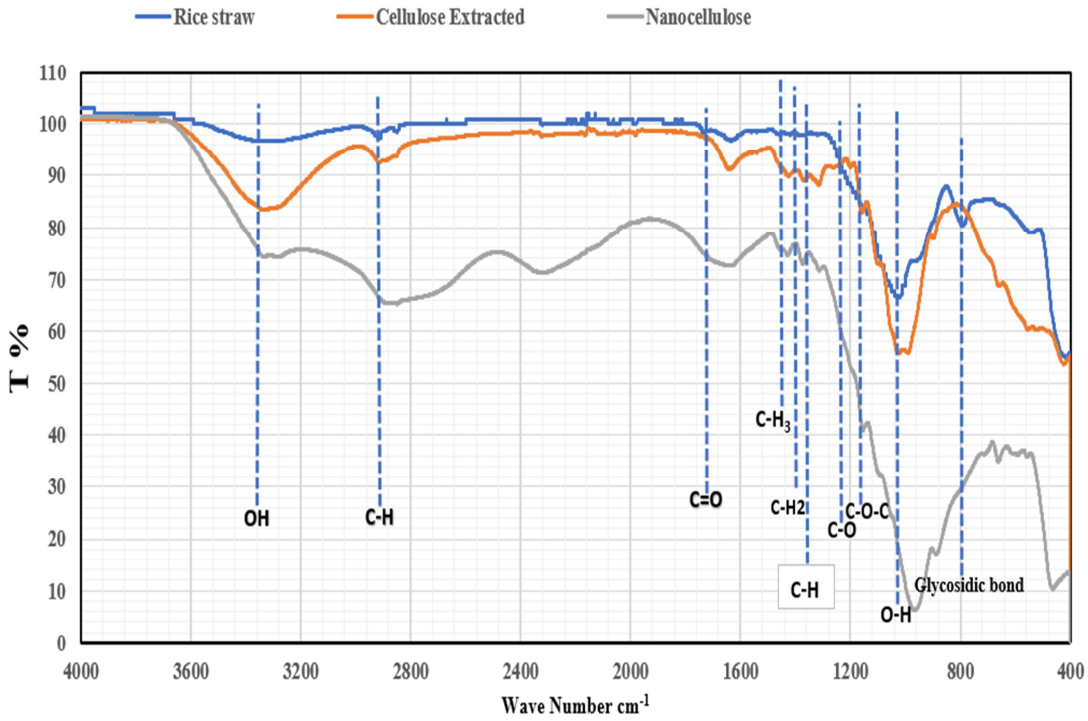

Figure 2: FT-IR Spectra of rice straw, extracted cellulose, and Nanocellulose

ii. Morphological study

Scanning electron microscopy (SEM) was utilized to investigate the structural characteristics of the materials (Figure 3). Images of raw rice straw revealed an intricate, interconnected fiber network with textured surfaces, typical of lignocellulosic biomass and attributed to lignin and hemicellulose presence [8]. Small, spherical protrusions, consistent with common silica formations in rice, were also observed on the fiber surfaces [42, 43]. Following alkaline and bleaching treatments designed for cellulose isolation, SEM depicted significant morphological changes in the rice straw fibers. The effective removal of lignin and hemicellulose yielded cellulose fibers that appeared as discrete, smoother strands compared to the untreated material [8, 42, 44, 45]. Further SEM analysis of the extracted nanocellulose (Figure 3) demonstrated a distinct rod-shaped morphology with smooth, elongated particles forming a dense, interconnected fibril network. This fibrillar arrangement is a key factor in the material's enhanced mechanical properties. SEM can also offer insights into material stability, as increased surface roughness under certain environmental conditions may suggest potential degradation of the nanocellulose structure.

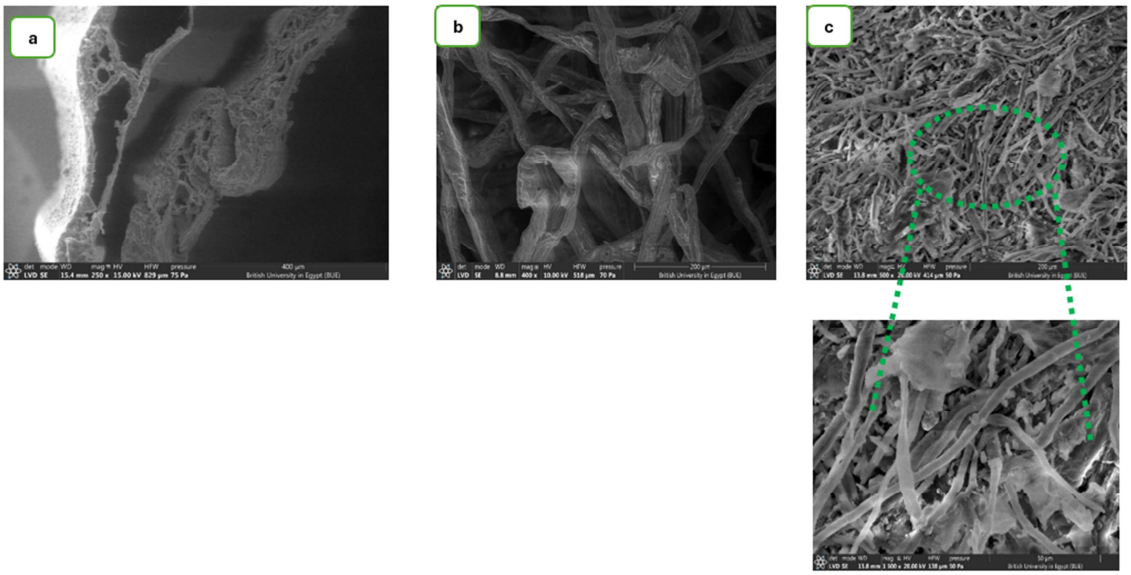

Figure 3: SEM images of **(a)** Rice straw, **(b)** Extracted cellulose, and **(c)** Nanocellulose

Transmission electron microscopy (TEM) was utilized to characterize the structural features of rice straw, extracted cellulose, and nanocellulose (NC). As seen in Figure 4, raw rice straw displayed a complex, heterogeneous structure typical of lignocellulosic materials, featuring large, irregularly shaped dark regions representing various components such as cellulose, hemicellulose, and lignin. Extracted cellulose, as shown in Figure 4, exhibited a more defined fibrous morphology. Individual cellulose particles appeared as dark, irregularly shaped aggregates forming a loose, network-like structure. TEM analysis, presented in **Figure 4**, confirmed that the nanocellulose particles isolated from rice straw were consistently **rod-shaped**, with dimensions ranging from 15 to 24 nm. This uniform morphology provides strong evidence for the efficacy of our extraction method, which effectively converted the raw cellulose into a high-aspect-ratio nanomaterial by isolating the crystalline cellulose regions during processing [42]. The resulting nanoscale dimensions and rod-like structure of the particles are expected to significantly enhance the mechanical strength, surface area, and overall reactivity when integrated into the final composite material, making them a superior reinforcing agent compared to untreated cellulose [44].

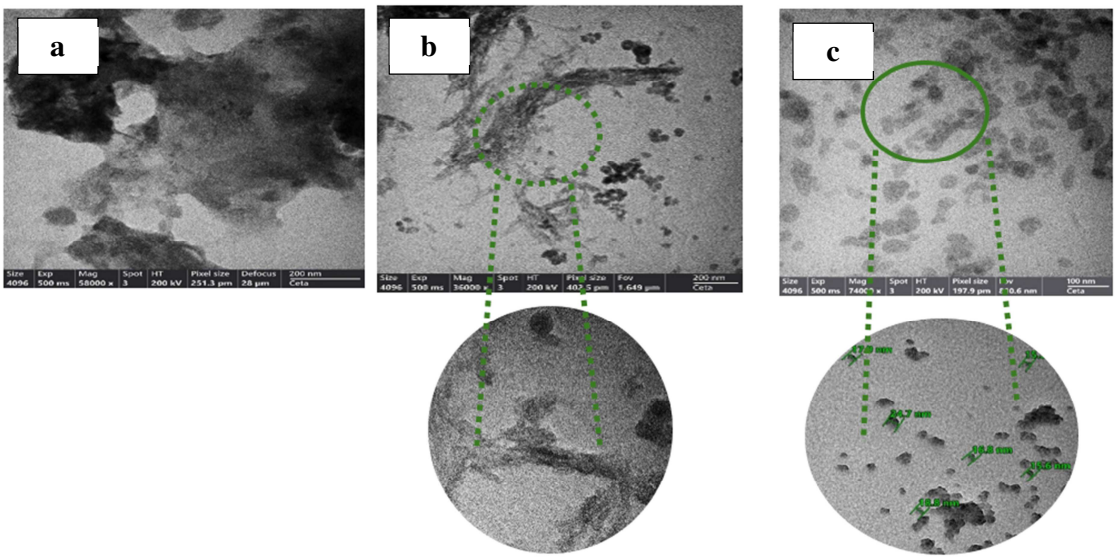

Figure 4: TEM images of: (**a)** Rice straw, **(b)** Cellulose, and **(c)** Nanocellulose

iii. Zeta potential and particle size analysis

Zeta potential, a measure of surface charge, is a key indicator of colloidal dispersion stability. Chemical treatments, such as oxidation or carboxylation, can enhance the negative zeta potential of rice straw to values between -40 and -60mV [46]. While cellulose from rice straw typically exhibits a zeta potential between -5 and -30mV, extensive chemical processing can increase its negative charge [47]. Nanocellulose, derived from plants or bacteria, naturally possesses a negative zeta potential due to its negatively charged surface, promoting dispersion stability. The specific zeta potential of nanocellulose varies based on its source, production method, and surface chemistry, ranging from -10 to -75mV. A more negative zeta potential generally indicates greater stability, with values above -30mV considered stable [46–48]. Chemical modification, pH adjustment, or surfactant addition can be used to manipulate zeta potential and control dispersion stability. The zeta potential measurements of rice straw, cellulose, and nanocellulose samples all indicate predominantly negative surface charges, as shown in Figure 5. The narrow, intense peaks centred around -44.8mV, -52.2mV, and -56.3mV, respectively, suggest homogeneous charge distributions. These negative zeta potentials contribute to the stability of the colloidal systems, preventing particle aggregation. The high peak intensities indicate abundant particles with these negative charges. Nanocellulose intrinsically has the most negative zeta potential due to its high surface area and surface charges. Understanding zeta potential is essential for optimizing nanocellulose processing and performance in various applications. Further analysis could reveal factors influencing zeta potential, such as particle size, as shown in Figure 6.

Particle size analysis of rice straw, cellulose, and nanocellulose revealed that all samples exhibited polydisperse distributions with varying characteristics (Figure 6).

For **rice straw**, the mean particle size was 2077.4nm, with a dominant peak observed at 4951.0nm. Its Z-average was 3408.7nm, and the polydispersity index (PI) was 1.062, indicating the broadest and most diverse particle size distribution among the samples.

Cellulose displayed a mean size of 639.5nm, a dominant peak at 228.0nm, a Z-average of 2626.9nm, and a PI of 0.962.

Finally, **nanocellulose** had a mean particle size of 221.7nm, a dominant peak at 283.7nm, a Z-average of 4106.4nm, and a PI of 1.965. Despite certain measurements indicating a broad spread, these results collectively suggest distinct size profiles for each processed material.

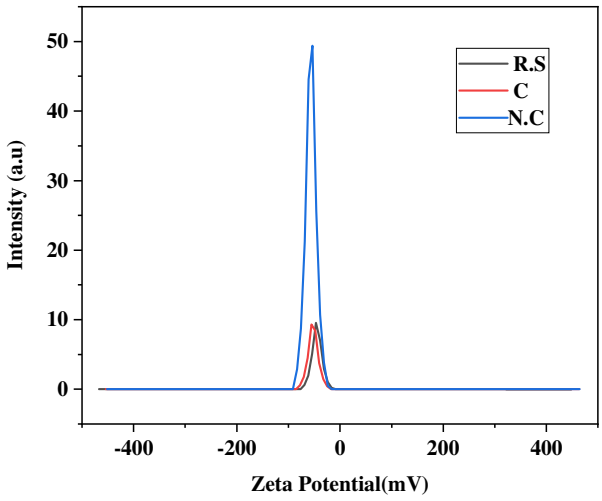

Figure 5: Zeta potential of rice straw, extracted cellulose, and Nanocellulose

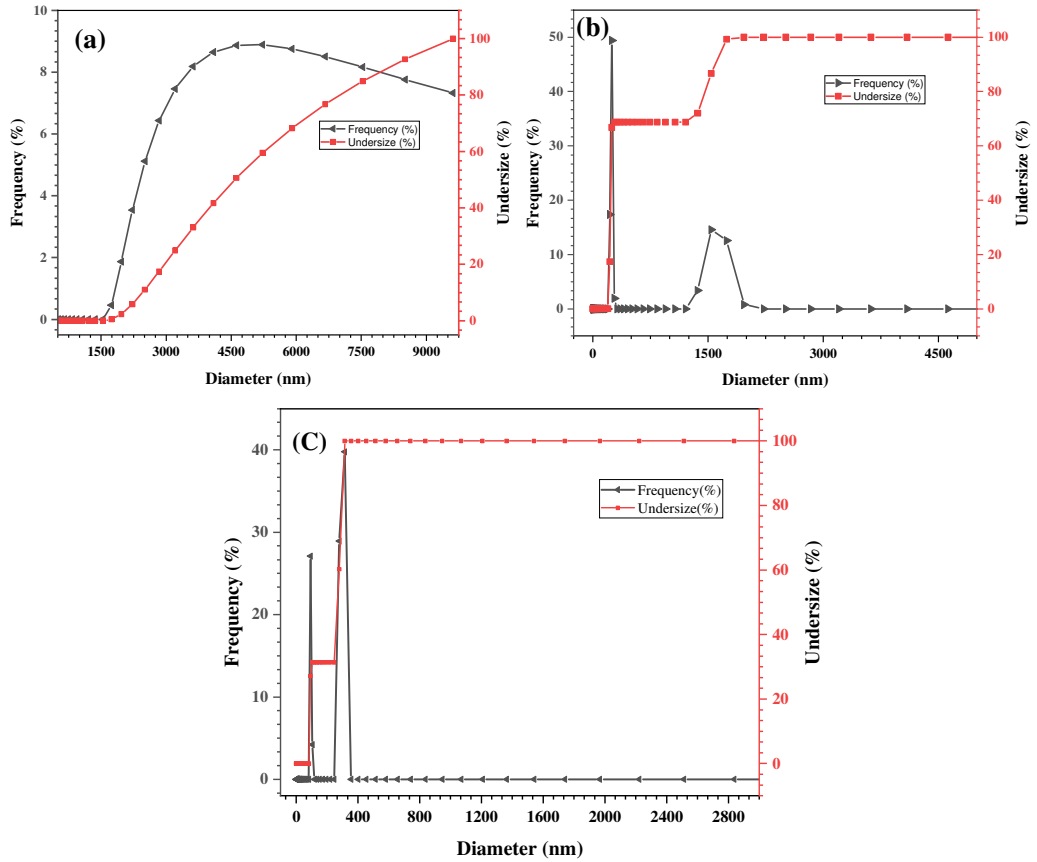

Figure 6: Particle size of: **a)** Rice straw, **b)** Extracted cellulose, and **c)** Nanocellulose

3.3. Characteristics of HDPE and HDPE/nanocellulose composite

3.3.1. FTIR spectrum of HDPE and HDPE/nanocellulose composite

Figure 7 and Table 3 exhibit the functional groups, their formed bonds, and their range for HDPE and HDPE/nanocellulose composite, analysed by means of Fourier transform infrared spectroscopy (FTIR). FTIR analysis of HDPE shows characteristic peaks related to its linear polyethylene structure (Figure 7). As seen in the FTIR spectra, the strong peaks at 2915 cm^{-1} and 2847 cm^{-1} are characteristic of the symmetric and asymmetric C-H stretching vibrations originating from the methylene groups ($-CH_2$) in the HDPE polymer backbone. These bands confirm that the nanocellulose was successfully incorporated into the HDPE matrix without altering the fundamental chemical structure of the polymer. The sharp bands at 1471cm^{-1} and 729cm^{-1} further support this observation, as they correspond to the methylene bending vibrations of HDPE. The presence of two bands at 730cm^{-1} and 720cm^{-1} suggests a highly crystalline nature [49]**.** The disappearance of the C=C band at 1600cm^{-1} in the polymerized spectrum confirms the formation of polyethylene from ethylene [49]**.** The FTIR spectrum of polyethylene is relatively simple due to its nonpolar and saturated nature, with few characteristic bands representing the methylene groups and the carbon backbone.

FTIR analysis of the HDPE/nanocellulose composite revealed characteristic peaks from both HDPE and nanocellulose (Figure 7). New bands attributed to nanocellulose, including a broad band around 3350-3408cm^{-1} due to O-H stretching and bands in the 1050-1300cm^{-1} region associated with C-O stretching, were observed. The composite spectrum exhibited changes in band intensity and shape compared to the individual components, suggesting interactions between HDPE and nanocellulose. The composite spectrum showed slight broadening of the methylene stretching bands at 2914cm^{-1} and 2847cm^{-1}, suggesting a decrease in crystallinity due to nanocellulose incorporation. Furthermore, reduced intensity of the bands associated with HDPE's crystalline structure (e.g., 729 and 718cm^{-1}) supported this decrease. This reduction in crystallinity could influence the composite's physical and mechanical properties. A weak broadband at 3371cm^{-1} was likely due to adsorbed moisture in the HDPE.

The FTIR analysis indicated that nanocellulose incorporation disrupted the regular polyethylene chain packing in the HDPE matrix, resulting in decreased crystallinity. This reduction could be attributed to interactions between HDPE and nanocellulose, potentially involving hydrogen bonding between nanocellulose hydroxyl groups and HDPE methylene groups or physical entanglements.

The FTIR analysis offered valuable insights into the chemical structure and interactions within the HDPE/nanocellulose composite, which could be correlated with its physical and mechanical properties. The observed decrease in crystallinity could potentially impact properties such as stiffness, strength, and thermal behaviour. Understanding and controlling these interactions are crucial for tailoring the material's performance.

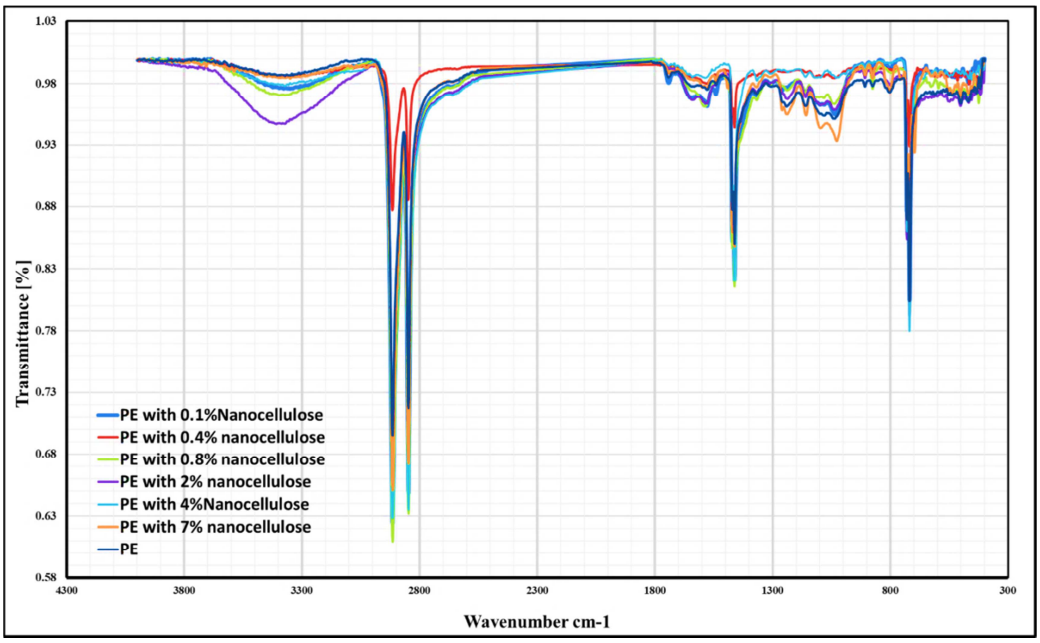

Figure 7: FTIR Spectrum of HDPE and HDPE/Nanocomposite

Table 3: FTIR Spectrum of HDPE and HDPE/Nanocomposite

	Function groups	PE blank	PE with 0.1% nanocellulose	PE with 0.4% nanocellulose	PE with 0.8% nanocellulose	PE with 2% nanocellulose	PE with 4% nanocellulose	PE with 7% nanocellulose	Appearance
		Wave number cm^{-1}							
PE from Re	C-H stretching vibrations of Methylene	2915	2914	2915	2914	2914	2914	2914	Slightly decrease
	C-H stretching vibrations of Methylene	2847	2847	2847	2847	2847	2847	2847	Slightly decrease
	Methylene (CH_2) bending vibrations	1471	1471	1471	1471	1471	1471	1471	Slightly decrease
	CH_2 bending vibrations	729	729	729	729	729	729	729	Slightly decrease

	C=C band disappearance of at 1600 cm^{-1}	-	-	-	-	-	-	-	Disappearance due to the polymerization reaction
Nanocellulose	A broad band is O-H stretching vibrations of hydroxyl groups in nanocellulose 3340 cm^{-1}	3373	3351	3373	3393	3408	3371	3350	Broads appear and increase with increase nanocellulose
	C-O stretching vibrations of the alcohol groups (C-O-H) in nanocellulose 1050-1300 cm^{-1}	-	1050 1260	1050 1260	1050 1238	1050 1236	1050 1241	1050 1239	Broad and increase with increase nanocellulose (4% -7%)
HDPE/Nanocellulose composite	Slightly broader of methylene stretching bands at 2915 cm^{-1} and 2847 cm^{-1}	-	2914-2847	2915-2847 (Decrease)	2914-2847	2914-2847	2914-2847	2914-2847	-
	Decrease of CH_2 bending vibrations 729 cm^{-1}) due to decrease in crystallinity	729 and 718	729 and 718	729 and 718	729 and 718	729 and 718	729 and 718	729 and 718	(Decrease slightly)

3.3.2. Thermogravimetric Analysis (TGA) of HDPE and HDPE/nanocellulose composite

The provided TGA curve illustrates the thermal degradation behaviour of various composite materials: HDPE (high-density polyethylene), HDPE/0.1% cellulose, HDPE/2% cellulose, and HDPE/7% cellulose (Figure 8). TGA is a technique used to measure the weight loss of a material as it is heated. All samples exhibited a slight initial weight loss around 100-150°C, likely due to the evaporation of moisture or other volatile components [50]. The primary weight loss for all samples occurred between 300 and 500°C, corresponding to the decomposition of the HDPE polymer chains. The HDPE/cellulose composites demonstrated slightly lower weight loss compared to pure HDPE in this temperature range, suggesting that the cellulose component may provide some thermal stability to the HDPE, consistent with previous studies [21, 51]**.** As the cellulose content increased in the composites, the overall weight loss during decomposition decreased, indicating that cellulose acts as a reinforcing filler, providing structural support and reducing the amount of HDPE that can decompose. The HDPE/7% cellulose composite exhibited the lowest weight loss, suggesting that a high cellulose content significantly enhances the thermal stability of the material [50]. After complete decomposition, a small residual weight remained for all samples, possibly due to inorganic components or char formation. The heating rate used in the TGA experiment can influence the curve's shape, and other factors, such as the particle size and distribution of the cellulose in the composite, impact the thermal properties, and consequently, these combined factors affect the overall thermal behaviour [21, 51]

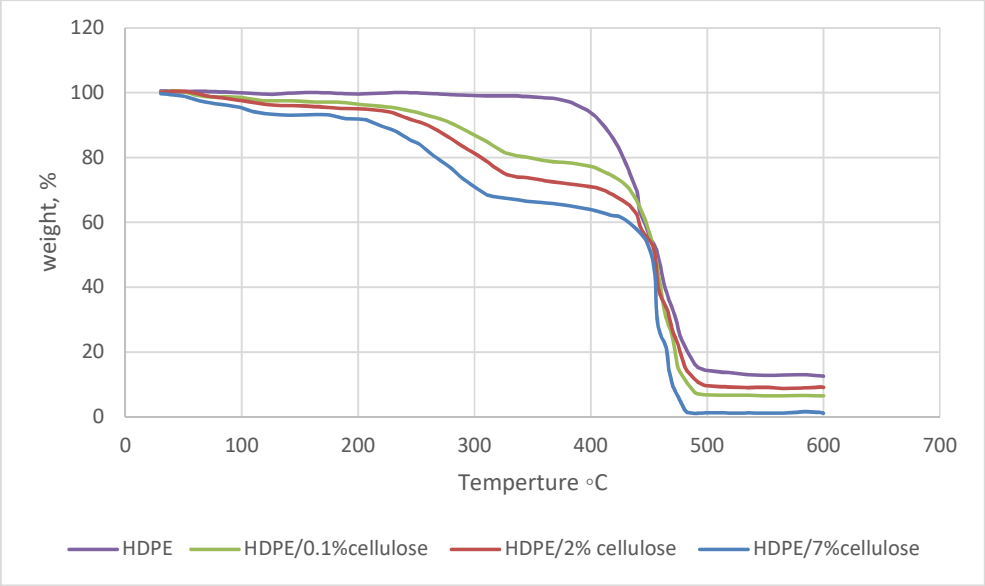

Figure 8: Thermogravimetric curves (TGA) for HDPE-NC composite

Figure 9 shows a derivative thermogravimetric analysis (DTG) curve for the same composite materials as in the previous TGA curve: HDPE, HDPE/0.1% Nanocellulose, HDPE/2% Nanocellulose, and HDPE/7% Nanocellulose. DTG is a technique that calculates the rate of weight loss during a TGA experiment. Peaks in the DTG curve indicate the temperature ranges where the most rapid weight loss occurs. The main peaks in the DTG curve correspond to the decomposition of the HDPE polymer chains, which occurs between 300 and 500°C. The shape and position of these peaks can provide information about the kinetics of the decomposition process. The DTG curves for the HDPE/cellulose composites show broader and less intense peaks compared to pure HDPE. This suggests that the presence of cellulose slows down the decomposition process [50]. As the cellulose content increases, the peaks become even broader and less intense, indicating a further reduction in the decomposition rate. The small peaks at higher temperatures (above 500°C) in the DTG curves of the composites might correspond to the decomposition of any residual cellulose or other components.

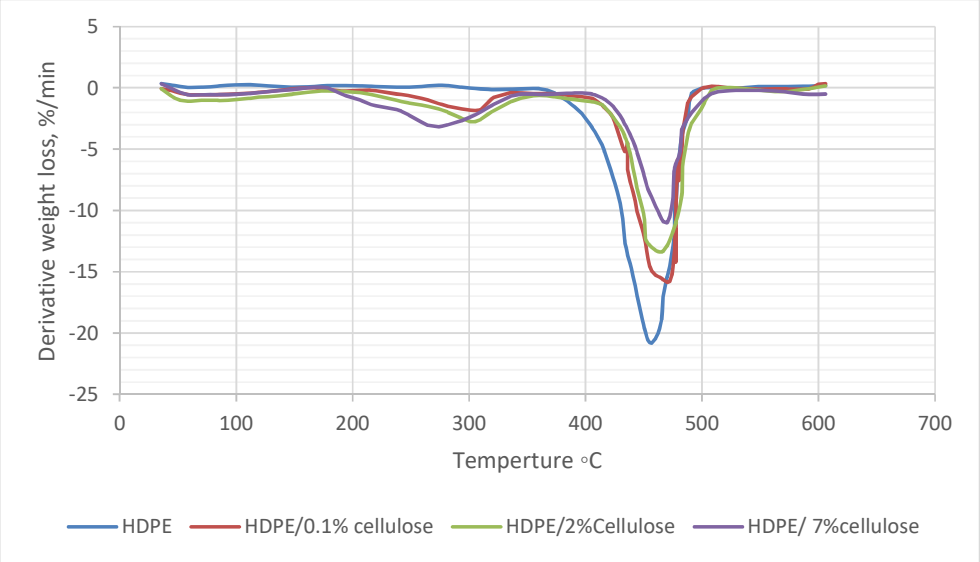

Figure 9: Derivative thermogravimetric (DTG) curves for HDPE-NC

3.3.3. Mechanical properties of HDPE and HDPE/nanocellulose composite

i. Tensile stress

Figure 10 depicts a bar graph illustrating the tensile stress of various HDPE/nanocellulose composite materials. Tensile stress, a measure of a material's maximum stress before breaking, is significantly enhanced in HDPE/nanocellulose composites compared to pure HDPE, indicating improved mechanical properties. As the nanocellulose content increases, the composite's tensile stress initially rises, suggesting that the nanocellulose acts as an effective reinforcing agent by forming strong interfacial bonds with the HDPE matrix [52, 53]. The improvement in tensile strength is a direct result of the reinforcing effect provided by the nanocellulose particles. This enhancement is facilitated by strong interfacial adhesion between the hydrophilic nanocellulose and the hydrophobic high-density polyethylene (HDPE) matrix. This robust interaction at the interface allows for the efficient transfer of mechanical stress from the polymer to the stiffer nanocellulose particles under an applied load, which prevents nanoparticle detachment and boosts the composite's overall mechanical performance.

At low nanocellulose concentrations, nanocellulose fibers act as reinforcing agents, improving tensile strength [53–55]. However, at higher concentrations, nanocellulose particles may agglomerate, leading to poor dispersion, reduced reinforcement, and interference with HDPE polymer chain alignment, potentially decreasing overall strength [49, 56]. An optimal nanocellulose content appears to be around 0.4% and 4%, where tensile stress reaches a maximum value. Beyond this point, further nanocellulose addition may decrease tensile stress due to factors like poor dispersion or interference with polymer chains [53, 54, 57].

Previous studies have reported that incorporating small amounts of nanocellulose (1-5 wt.%) into high-density polyethylene (HDPE) can significantly enhance its tensile stress, with increases ranging from 15% to 35% [58]. The addition of nanocellulose to HDPE provided reinforcement due to its high surface area, which facilitated interaction with the HDPE matrix through intermolecular hydrogen bonding, leading to increased tensile stress.

As illustrated in Figure 10 and Table 4, the incorporation of nanocellulose into HDPE resulted in a significant increase in tensile stress. Specifically, a 11.6% increase (22.5 MPa) was observed at 0.1 wt.% loading, a 14.38% increase (23.06MPa) at 0.4 wt.%, a 5.45% increase (21.26 MPa) at 0.8 wt.%, and a 12.45% increase (22.67MPa) at 4 wt.%. However, at 2 wt.% loading, a 10.67% decrease (17.99MPa) in tensile stress was noted, and at 7 wt.% loading, an 8.48% decrease (22.67MPa) was observed. The initial increase in tensile stress at low nanocellulose loadings can be attributed to the reinforcing effect of the nanocellulose fibers or crystals. The high surface area and aspect ratio of nanocellulose promote effective stress transfer from the HDPE matrix to the reinforcing phase, resulting in improved tensile properties. Additionally, nanocellulose can act as a nucleating agent, promoting the formation of smaller and more uniform crystalline structures in the HDPE matrix, further enhancing tensile strength [56]. However, as nanocellulose loading increases beyond a certain level, tensile strength starts to decline due to the agglomeration of nanocellulose particles. At higher loadings, nanocellulose particles tend to aggregate, forming clusters or agglomerates within the HDPE matrix [53, 55]. These agglomerates act as stress concentration points, leading to premature failure and a decrease in overall tensile strength [49]. Moreover, poor dispersion and inadequate interfacial adhesion between nanocellulose and the HDPE matrix at higher loadings can also contribute to the decline in tensile properties [58].

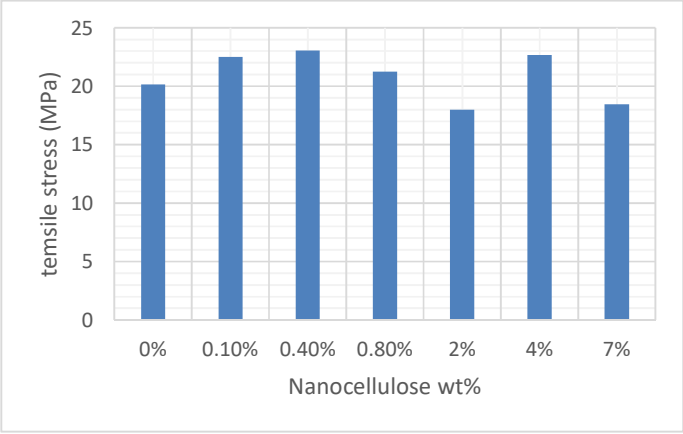

Figure 10: Tensile stress of HDPE/nanocellulose composites

Table 4: Tensile stress of HDPE/nanocellulose composites

Nanocellulose wt. %	Tensile stress	Study the effect %
Blank 0%	20.16	-
0.1%	22.5	+11.6
0.4%	23.06	+14.38
0.8%	21.26	+5.45
2%	17.99	-10.67
4%	22.67	+12.45
7%	18.45	-8.48

ii. Modulus:

Modulus, a measure of a material's stiffness, quantifies its resistance to elastic deformation under stress. Young's modulus, a common type, relates stress to strain within the elastic region. Higher Young's modulus signifies greater stiffness, requiring more force for the same deformation [49, 52, 55, 59]. Figure 11 illustrates the relationship between composition percentage and modulus (MPa) for the investigated composites. As composition increases from 0% to 0.40%, the modulus rises. A slight decrease occurs at 0.80%, followed by an increase to a peak at 4%, then a decline. At 0% composition, the modulus is approximately 600MPa. It reaches a maximum value of around 800MPa at 4% composition. At 7% composition, the modulus drops back to approximately 650MPa. This initial increase suggests reinforcement from the added component, while the peak at 4% indicates optimal composition for maximum stiffness. The subsequent decrease might be due to factors like increased porosity or weaker interfacial bonding [49, 57].

HDPE nanocomposites exhibit significant elastic modulus improvements due to stiff nanocellulose particles restricting the mobility and deformability of HDPE chains [57, 59]. This restriction enhances the material's resistance to deformation under stress. As nanocellulose content increases, the modulus improves due to the reinforcing effect of the rigid nanocellulose particles. However, this increased stiffness comes at the cost of reduced ductility. Additionally, the orientation of nanofibers along the tensile axis contributes to further stiffness enhancements by efficiently transferring the applied load [55, 59].

Our experimental study, as detailed in Figure 11 and Table 5, revealed substantial increases in the elastic modulus with nanocellulose incorporation: a 14.15% increase (672.21MPa) at 0.1% loading, a 31.50% increase (774.84MPa) at 0.4%, a 0.64% increase (593.02MPa) at 2%, a 17.38% increase (691.67MPa) at 4%, a decrease of 7.78% (543.36MPa) at 0.8%, and a 12.64% increase (663.74MPa) at 7% loading. The initial modulus increases at lower nanocellulose loadings (up to 0.4%) is attributed to the effective reinforcement from well-dispersed nanocellulose particles. These stiff fillers hinder chain movement, leading to increased resistance to elastic deformation and a higher modulus [59]. However, at higher loadings (0.8% and above), agglomeration and poor dispersion of nanocellulose particles can reduce reinforcing efficiency and lead to a decrease in elastic modulus, as observed at 0.8% loading. The stiff and rigid nature of nanocellulose particles plays a crucial role in restricting chain mobility and deformation, contributing to the observed modulus increases [54, 55, 59]. While these modulus enhancements are beneficial for certain applications requiring high stiffness, the accompanying decrease in ductility may limit the material's suitability for applications demanding flexibility or toughness. Therefore, optimizing nanocellulose loading and dispersion is crucial to achieve the desired balance between stiffness and ductility for specific applications.

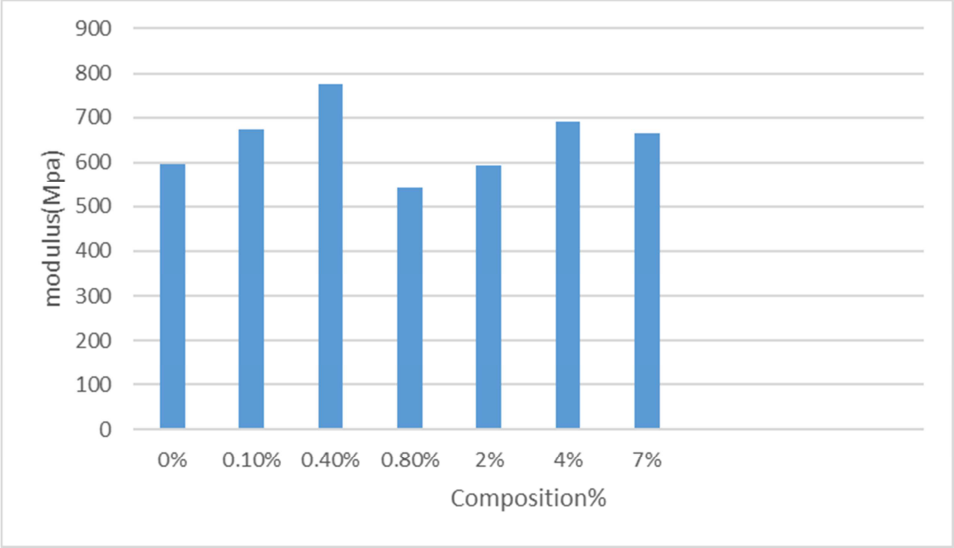

Figure 11: Modulus of HDPE/nanocellulose composites

Table 5: Modulus of HDPE/nanocellulose composites

Nanocellulose wt. %	Young modulus	Study the effect %
Blank 0%	589.21	-
0.1%	672.63	14.15 (+)
0.4%	774.84	31.50 (+)
0.8%	543.36	7.78 (-)
2%	593.02	0.64 (+)
4%	691.67	17.38 (+)
7%	663.74	12.64 (-)

iii. Elongation:

Elongation at break, a measure of a material's stretchability, is crucial for HDPE and its nanocellulose composites [49, 52, 55]. While pure HDPE exhibits high ductility, the incorporation of nanocellulose can significantly impact this property. Figure 12 presents a bar graph illustrating the relationship between the composition percentage of the investigated composites and their corresponding elongation (measured in mm). As shown in Figure 12, increasing nanocellulose content generally increases elongation, suggesting improved ductility. However, this trend is not linear. The initial increase in elongation with increasing composition could be due to the reinforcing effect of the added nanocellulose, which might improve the material's ability to stretch without breaking [52, 53, 60]. At 0.40% composition, a significant drop in elongation is observed, likely due to factors like poor dispersion or adverse interactions with the base material. The highest elongation is achieved at 4%, indicating an optimal balance between reinforcement and potential negative effects. Beyond 4%, a slight decrease in elongation is observed at 7%, possibly indicating a limit to the material's elongation capacity. While low nanocellulose loadings can increase elongation due to reinforcement, higher loadings or poor dispersion can decrease elongation due to restricted chain mobility and stress concentration points [52, 53, 60]. Strong interfacial adhesion can improve elongation by enhancing stress transfer. Balancing ductility with other improved mechanical properties requires careful optimization of nanocellulose loading and dispersion for specific applications.

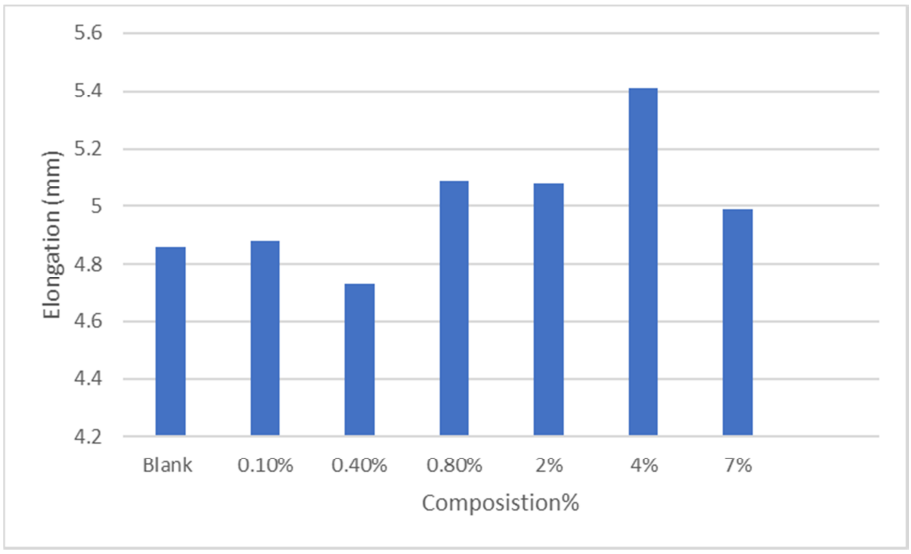

Figure 12: Elongation of HDPE/nanocellulose composites

iv. Yield point:

Figure 13 illustrates the relationship between the composition percentage of nanocellulose in HDPE/nanocellulose composites and the resulting yield strength of the material. The yield strength is a measure of the material's resistance to plastic deformation under stress [61, 62].

As illustrated in Figure 13 and Table 6, the incorporation of Nanocellulose (NC) into HDPE has been observed to increase the yield point by up to 30-40% compared to pure HDPE, depending on the nanocellulose loading level and dispersion quality. As the nanocellulose content increases from 0% to 4%, the yield strength of the composite also increases. This is likely due to the reinforcing effect of the nanocellulose particles, which hinder the movement of polymer chains and increase the material's resistance to deformation [62]. The highest yield strength is observed at 4% nanocellulose content, indicating an optimal balance between reinforcement and potential negative effects of excessive nanocellulose loading. This suggests that at this composition, the reinforcing effect of nanocellulose is maximized, leading to the highest resistance to plastic deformation.

Beyond 4%, the yield strength starts to decrease. This could be attributed to factors such as poor dispersion of nanocellulose particles at higher loadings, leading to agglomeration and reduced reinforcement efficiency [61, 62]. Additionally, excessive nanocellulose content might interfere with the polymer chain mobility, negatively impacting the material's mechanical properties.

Overall, the figure demonstrates that the addition of nanocellulose can significantly enhance the yield strength of HDPE composites, but careful optimization of the nanocellulose content is crucial to achieve the desired mechanical properties.

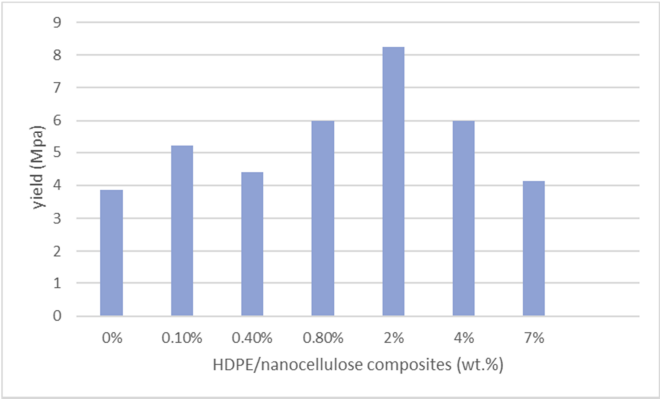

Figure 13: Yield point of HDPE/nanocellulose composites (wt.%)

Table 6: Yield point of HDPE/nanocellulose composites (wt.%)

HDPE/nanocellulose composites (wt.%)	Yield (KN)	Yield (Mpa)
Blank	0.29	3.86
0.1%	0.39	5.2
0.4%	0.33	4.4
0.8%	0.45	6
2%	0.62	8.26
4%	0.45	6
7%	0.31	4.13

3.3.4. Biodegradation of HDPE and HDPE/nanocellulose composite in the soil

As detailed in Table 7, the HDPE nanocomposites exhibited an initial weight gain during the first month of exposure to the soil environment. This increase, ranging from 0.058% to 0.17%, is attributed to the hydrophilic nature of nanocellulose, which readily absorbs moisture from the surrounding air and soil. While HDPE is generally hydrophobic, it can still absorb some moisture, especially in humid conditions [63].

In the second month, the blank HDPE and 0.1 wt.% nanocellulose composite experienced a slight weight decrease, likely due to the leaching of small nanocellulose fragments resulting from initial degradation. Conversely, composites with higher nanocellulose loadings (0.8-7 wt.%) continued to gain weight, indicating that moisture absorption outweighed degradation effects [14].

To account for the initial moisture absorption, weight loss measurements from the third month onwards were calculated relative to the first month. The 0.1-2 wt.% nanocellulose composites showed weight losses ranging from 0.096% to 0.181%, indicating degradation of the nanocellulose phase. In contrast, the 4 wt.% and 7 wt.% composites still exhibited slight weight gains, suggesting that moisture absorption dominated over degradation at these higher loadings. After 4 months, the 0.1-2 wt.% composites continued to lose weight due to ongoing degradation, while the 4 wt.% composite showed a weight loss of 0.18%. The 7 wt.% composite, despite a slight overall weight gain, also experienced a weight loss of 0.28% after accounting for moisture absorption, highlighting the complex interplay between degradation and moisture absorption [62].

The initial weight gain of all nanocomposites can be attributed to the hydrophilic nature of nanocellulose, which draws moisture from the soil. This effect is more pronounced at higher nanocellulose loadings due to the increased proportion of hydrophilic components. The subsequent weight loss, particularly at lower nanocellulose loadings, is primarily due to the biodegradation of the nanocellulose phase by microorganisms and enzymes present in the soil. The formation and leaching of smaller nanocellulose fragments contribute to this weight loss.

Interestingly, at the highest 7 wt.% nanocellulose loading, the moisture absorption effect still dominated over degradation even after 5 months. This suggests that above a certain nanocellulose threshold, the hydrophilicity of the material overshadows the degradation process within the studied timeframe [62].

Table 7: Biodegradation of HPDE/Nanocellulose composite

Nanocellulose wt. %	Blank	0.10%	0.40%	0.80%	2%	4%	7%
Time	Weight in grams						
Zero time	8.579	13.79	11.447	14.593	13.63	12.35	9.199
1st Month	8.584	13.81	11.456	14.618	13.65	12.37	9.214
2nd Month	8.574	13.77	11.447	14.607	13.66	12.39	9.245
3rd Month	8.573	13.785	11.445	14.603	13.648	12.384	9.237
4th Month	8.570	13.793	11.442	14.599	13.641	12.367	9.219
5th Month	8.570	13.786	11.442	14.599	13.640	12.367	9.219

The physical degradation of the nanocomposite surfaces was also evident from SEM images, as shown in Figure 14, which showed surface roughening after 5 months of soil exposure. This corroborates the weight loss data and indicates the degradation of the nanocellulose component.

While HDPE itself is non-biodegradable, the incorporation of nanocellulose into HDPE matrices can induce biodegradation behaviour, with the extent of degradation depending on the nanocellulose content and exposure conditions [62].

The provided SEM images offer insights into the microstructure of a polymer composite material. Figure 14 (a) reveals a relatively smooth surface with a potential fracture, indicating a post-processing or inherent material characteristic. Figure 14 (b) showcases a fibrous structure with fiber bundles and pores, suggesting a composite material with potential non-uniform fiber distribution. Figure 14 (c), a cross-sectional view, reveals the interface between the matrix and fibers, indicating a relatively uniform fiber distribution. The presence of fibers enhances mechanical properties, while porosity and non-uniform fiber distribution may influence performance [60, 62].

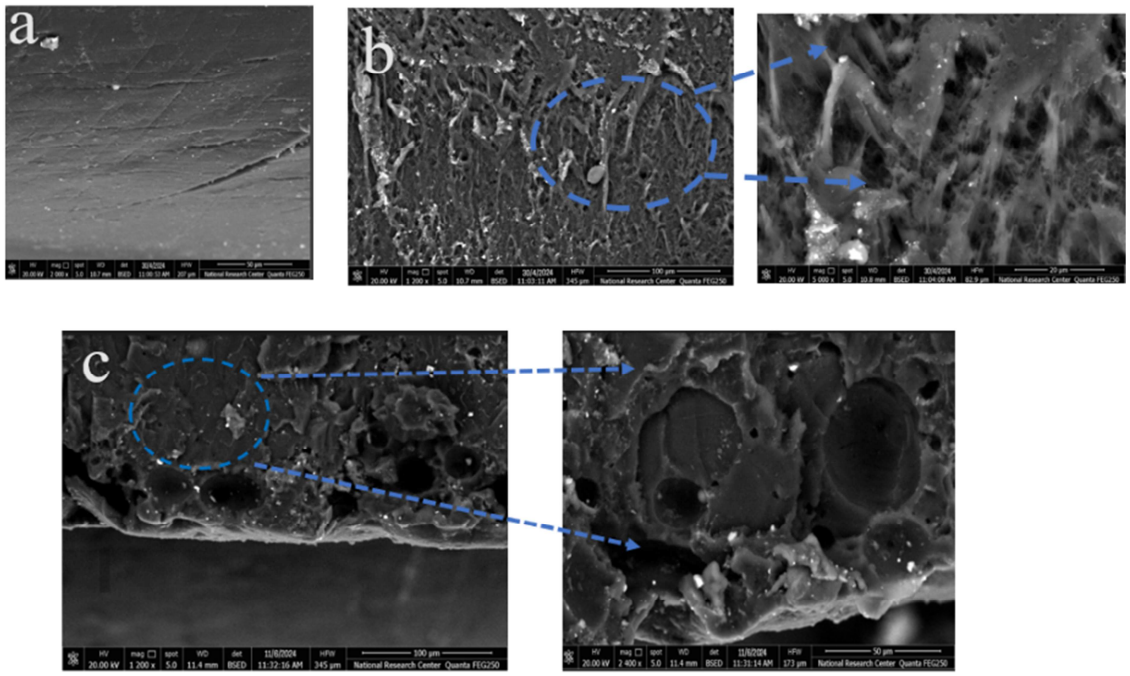

Figure 14: SEM image of HDPE: **(a)** Blank **(b)** with 7wt.% nanocellulose before degradation **(c)**after degradation

4. Comparison of existing outcomes with other outcomes

A comparison of existing outcomes with other consequences for utilizing rice straw-derived nanocellulose to enhance HDPEs' mechanical, thermal, and biodegradation properties, surpassing previous works in sustainability and performance, is exhibited in Table 8. Compared to other nanocomposites, it offers a renewable, scalable, and eco-friendly solution with superior dispersion and partial biodegradability.

Table 8: Differentiation between existing outcomes with earlier consequences

Comparison	This study	Study 1 [53]	Study 2 [64]	Study 3 [58]
Base Polymer	High-Density Polyethylene (HDPE)	Polylactic Acid (PLA)	PLA	(HDPE) and Maleic Anhydride-Grafted High-Density Polyethylene (HDPE-g-MA).
Reinforcing Material	Nanocellulose from rice straw (agricultural waste)	Microcrystalline Cellulose (MCC)	Two nano reinforcements were used: bentonite (a layered silicate) and microcrystalline cellulose (MCC).	$M_2(HT)_2$ Organoclay (modified montmorillonite) was used as the reinforcing material.
Processing Method	Melt mixing using Brabender + hot pressing	Twin-screw extrusion followed by injection molding.	solution casting**,** with pre-treatment of nano reinforcements	Melt-processing technique involved the use of a twin-screw extruder
Fiber/Particle Size	4.49–8.43nm (measured by TEM)	MCC Size: 10-15µm (particulate form). Wood Flour (WF) Size: 150-750µm (coarse powder). Wood Pulp (WP) Size: 20-30µm (fibrous pellets).	Bentonite (Layered Silicate): Sheet dimensions: 800 × 800 × 1nm Microcrystalline Cellulose (MCC): MCC consists of aggregated cellulose microcrystals. After processing (swelling,	315.6nm (at 0% HDPE-g-MA) to 55.5nm (at 100% HDPE-g-MA).

Comparison	This study	Study 1 [53]	Study 2 [64]	Study 3 [58]
			freeze-drying, redispersion), the MCC formed sheet-like agglomerates rather than exfoliated whiskers.	
Tensile Strength Improvement	+14.38% at 0.4wt% nanocellulose	Decreased with MCC; better in WF and WP	PLA/bentonite showed a 47% increase in yield strength, whereas PLA/S-MCC showed only a 12% increase.	It increases with the addition of montmorillonite and small amounts of HDPE-g-MA, levelling off at certain HDPE-g-MA contents (15-25%).
Elastic Modulus Improvement	+31.50% at 0.4 wt%	Increased with MCC; highest in WF and WP composites	A 53% increase in tensile modulus was observed with bentonite, while MCC provided no improvement.	It improves significantly with increased montmorillonite content but levels off at higher HDPE-g-MA contents (> 50%)
Biodegradability	Partial degradation observed after 5 months (soil burial test)	Enhanced in WF composites; MCC composites are less biodegradable.	PLA is biodegradable, and while MCC is biodegradable and renewable, bentonite is not biodegradable.	Not studied
Key Distinction	Renewable source, dual improvement (mechanical + thermal), partial biodegradation	WF provides a balance of strong mechanical properties and biodegradability, while MCC offers limited biodegradability despite some mechanical benefits.	Bentonite provided superior mechanical and barrier properties, but MCC offers a fully renewable and biodegradable alternative.	Modest property improvement, no sustainability focus

5. Conclusions

This study successfully developed eco-friendly nanocomposites by incorporating rice straw-derived nanocellulose into high-density polyethylene (HDPE). Nanocellulose, extracted from rice straw through alkaline pulping, bleaching, and acid hydrolysis, had diameters ranging from 15 to 24nm and a stable zeta potential of -50.8mV, indicating good dispersion. The resulting HDPE/nanocellulose composites exhibited enhanced mechanical properties, with optimal performance at 0.4-0.8 wt% nanocellulose loading. Tensile strength increased by up to 14.38%, Young's modulus improved by up to 31.50%, and yield strength rose substantially. While elongation at break generally decreased, the balance between strength and ductility was maintained.

Thermogravimetric analysis revealed that the nanocomposites exhibited a two-step degradation process. The initial step (around 227-341°C) was attributed to the decomposition of the cellulosic component, while the second (around 430°C) was due to HDPE degradation. Soil burial tests conducted over five months indicated the biodegradation of the nanocellulose component, as evidenced by weight loss and changes in surface morphology observed through scanning electron microscopy (SEM). To account for potential moisture absorption effects, weight loss measurements after the third month were normalized to the initial weight. At the conclusion of the five months, weight losses ranged from 0.163-0.129 wt.% for the 0.1-2 wt.% nanocellulose composites. The 4 wt.% and 7 wt.% composites exhibited weight losses of 0.18% and 0.28%, respectively.

These results highlight the potential of rice straw-derived nanocellulose as an effective reinforcing agent for HDPE, offering a pathway to develop more sustainable composite materials. The partial biodegradability observed in the nanocomposites suggests a potential reduction in environmental impact compared to conventional HDPE products.

By demonstrating a viable method for valorizing agricultural waste and enhancing the properties of a common polymer, this study makes a significant contribution to sustainable materials science. The development of these nanocomposites offers a promising solution for both plastic waste and agricultural residue, aligning with circular economy principles by turning waste into valuable products with superior characteristics. Building on these findings, future work should focus on optimizing the

long-term biodegradability of these composites and exploring their potential for industrial applications. Specifically, we recommend investigating the use of compatibilizers to improve performance, assessing the feasibility of scaling up production, and conducting a detailed study on biodegradability under controlled industrial composting conditions.

6. Conflicts of interest

"There are no conflicts to declare".

7. Formation of funding sources

No funding was received for this study.

8. References

1. Volk N, He R, Magniez K (2015) Enhanced homogeneity and interfacial compatibility in melt-extruded cellulose nano-fibers reinforced polyethylene via surface adsorption of poly (ethylene glycol)-block-poly (ethylene) amphiphiles. Eur Polym J 72:270–281
2. Yasim-Anuar TAT, Ariffin H, Norrrahim MNF, Hassan MA, Tsukegi T, Nishida H (2019) Sustainable one-pot process for the production of cellulose nanofiber and polyethylene/cellulose nanofiber composites. J Clean Prod 207:590–599
3. Riseh RS, Vazvani MG, Hassanisaadi M, Thakur VK (2024) Agricultural wastes: A practical and potential source for the isolation and preparation of cellulose and application in agriculture and different industries. Ind Crops Prod 208:117904
4. Satlewal A, Agrawal R, Bhagia S, Das P, Ragauskas AJ (2018) Rice straw as a feedstock for biofuels: availability, recalcitrance, and chemical properties. Biofuels, Bioprod Biorefining 12:83–107
5. Nasir M, Hashim R, Sulaiman O, Asim M (2017) Nanocellulose: Preparation methods and applications. In: Cellulose-reinforced nanofibre composites. Elsevier, pp 261–276
6. Nasir M, Hashim R, Sulaiman O, Nordin NA, Lamaming J, Asim M (2015) Laccase, an Emerging Tool to Fabricate Green Composites: A Review. BioResources 10:
7. Goodman BA (2020) Utilization of waste straw and husks from rice production: A review. J Bioresour Bioprod 5:143–162
8. Sharma N, Allardyce BJ, Rajkhowa R, Agrawal R (2023) Rice straw-derived cellulose: a comparative study of various pre-treatment technologies and its conversion to nanofibres. Sci Rep 13:16327
9. Singh Y, Sharma S, Kumar U, Sihag P, Balyan P, Singh KP, Dhankher OP (2023) Strategies for economic utilization of rice straw residues into value-added by-products and prevention of environmental pollution. Sci Total Environ 167714
10. Laftah WA, Wan Abdul Rahman WA (2021) Rice waste–based polymer composites for packaging applications: A review. Polym Polym Compos 29:S1621–S1629
11. Ibrahim N (2023) "Recycling rice straw as a type of agricultural solid waste" Alternatives of using rice straw in Building construction as a tool to protect the environment in Egypt. MSA Eng J 2:100–132
12. Mohamed R, Abu Hashish H, Ahmed H, Awad M, Kadry G (2022) A competent, humble cost catalyst from biowaste: high performance and combustion characteristics of alternative diesel fuel. Egypt J Chem 65:265–277
13. Awydat H, Abdelwahed FT, El-Sayed NS, El Defrawy MM, Eltabey RM (2025) Valorization of Sugarcane Bagasse into Cellulose Nanofibers for Efficient Adsorption of Chromium Hexavalent Ions. Egypt J Chem 68:1–10
14. Kadry G, Abd El-Hakim AEF (2015) Effect of nanocellulose on the biodegradation, morphology and mechanical properties of polyvinylchloride/nanocellulose nanocomposites. Res J Pharm Biol Chem Sci 6:659–666
15. Marcovich NE, Auad ML, Bellesi NE, Nutt SR, Aranguren MI (2006) Cellulose micro/nanocrystals reinforced polyurethane. J Mater Res 21:870–881
16. Oun AA, Rhim J-W (2016) Characterization of nanocelluloses isolated from Ushar (Calotropis procera) seed fiber: Effect of isolation method. Mater Lett 168:146–150
17. Osong SH, Norgren S, Engstrand P (2016) Processing of wood-based microfibrillated cellulose and nanofibrillated cellulose, and applications relating to papermaking: a review. Cellulose 23:93–123
18. Habibi Y, Lucia LA, Rojas OJ (2010) Cellulose nanocrystals: chemistry, self-assembly, and applications. Chem Rev 110:3479–3500
19. Miao C, Hamad WY (2013) Cellulose reinforced polymer composites and nanocomposites: a critical review. Cellulose 20:2221–2262
20. Khalil HPSA, Bhat AH, Yusra AFI (2012) Green composites from sustainable cellulose nanofibrils: A review. Carbohydr Polym 87:963–979
21. Tajeddin B, Abdulah LC (2010) Thermal properties of high density polyethylene-kenaf cellulose composites. Polym Polym Compos 18:257–261
22. Li X, Tabil LG, Oguocha IN, Panigrahi S (2008) Thermal diffusivity, thermal conductivity, and specific heat of flax fiber–HDPE biocomposites at processing temperatures. Compos Sci Technol 68:1753–1758
23. Zhang MQ, Rong MZ, Lu X (2005) Fully biodegradable natural fiber composites from renewable resources: all-plant fiber composites. Compos Sci Technol 65:2514–2525
24. Pedro J, Franco H, Gonzalez A V (2005) Fibre-matrix adhesion in natural fibre composites. Nat fibres, Biopolym biocomposites Taylor Fr Boca Raton, Florida 177–230
25. Jayasekara R, Harding I, Bowater I, Christie GBY, Lonergan GT (2004) Preparation, surface modification and characterisation of solution cast starch PVA blended films. Polym Test 23:17–27

26. Kroon M, Hagman A, Petersson V, Andreasson E, Almström M, Jutemar EP (2024) Impact testing of high-density polyethylene structure. Int J Impact Eng 105033
27. ASTM D (2009) 2854-09. Standard test method for apparent density of activated carbon. ASTM Stand 96:1–3
28. Aragaw T, Leta S, Alayu E, Mekonnen A (2022) Chromium Removal from Electroplating Wastewater Using Activated Coffee Husk Carbon. Adsorpt Sci Technol 2022:
29. El-Gawad HA, Kadry G, Zahran HA, Hussein MH (2023) Chromium Disarmament from Veritable Tanneries Sewer Water Utilizing Carbonic Rice Straw as a Sorbent: Optimization and Carbonic Rice Straw Characteristics. Water, Air, Soil Pollut 234:659
30. Archanowicz E, Kowaluk G, Niedziński W, Beer P (2013) Properties of particleboards made of biocomponents from fibrous chips for FEM modeling. BioResources 8:6220–6230
31. Ismail I, Jalil Z, Fadzullah SH (2019) Mechanical and physical properties of rice straw fiber-reinforced polypropylene composite. In: IOP Conference Series: Earth and Environmental Science. IOP Publishing, p 12013
32. Amin GA, Kadry GA, Razek T, Hassabo AG (2025) Fabrication and characterization of rice straw-derived cellulose nanofibers for enhanced adsorption of reactive black 5 and methylene blue dyes from aqueous solutions. Egypt J Chem 68:653–672
33. Heavner DL, Morgan WT, Ogden MW (1996) Determination of volatile organic compounds and respirable suspended particulate matter in New Jersey and Pennsylvania homes and workplaces. Environ Int 22:159–183
34. Muliarta IN (2019) A study on rice field farmer implementation of rice straw composting. In: IOP Conference Series: Earth and Environmental Science. IOP Publishing, p 12001
35. Konttinen YT, Xu J-W, Pätiälä H, Imai S, Waris V, Li T-F, Goodman SB, Nordsletten L, Santavirta S (1997) Cytokines in aseptic loosening of total hip replacement. Curr Orthop 11:40–47
36. Poornejad N, Karimi K, Behzad T (2013) Improvement of saccharification and ethanol production from rice straw by NMMO and [BMIM][OAc] pretreatments. Ind Crops Prod 41:408–413
37. Bhattacharyya P, Bhaduri D, Adak T, Munda S, Satapathy BS, Dash PK, Padhy SR, Pattanayak A, Routray S, Chakraborti M (2020) Characterization of rice straw from major cultivars for best alternative industrial uses to cutoff the menace of straw burning. Ind Crops Prod 143:111919
38. Abd El Gawad HA, Zahran H (2023) Silver withdrawal from X-Ray waste via leaching and sorption techniques: Appraisal ideal treatment factors. Egypt J Chem 66:509–522
39. Abderrahim B, Abderrahman E, Mohamed A, Fatima T, Abdesselam T, Krim O (2015) Kinetic thermal degradation of cellulose, polybutylene succinate and a green composite: comparative study. World J Environ Eng 3:95–110
40. Abou El Fettouh Abd El-Hakimb a and Ghada Kadry b*. (2019) Improvement of saccharification and ethanol production from rice straw by NMMO and [BMIM][OAc] pretreatments. Res J Pharm Biol Chem Sci 10(3):11
41. Wulandari WT, Rochliadi A, Arcana IM (2016) Nanocellulose prepared by acid hydrolysis of isolated cellulose from sugarcane bagasse. In: IOP conference series: materials science and engineering. IOP Publishing, p 12045
42. El-Zawahry MM, Hassabo AG, Mohamed AL (2023) Preparation of cellulose gel extracted from rice straw and its application for metal ion removal from aqueous solutions. Int J Biol Macromol 248:125940
43. Kamboj R, Bains A, Sharma M, Kumar A, Ali N, Parvez MK, Chawla P, Sridhar K (2024) Green synthesis of rice straw-derived silica nanoparticles by hydrothermal process for antimicrobial properties and effective degradation of dyes. Process Saf Environ Prot 185:1049–1060
44. Yassine BA, Bezbiz M, Belachemi L, Moreau C, Garnier C, Jonchere C, Cathala B, Kaddami H (2024) Preparation of superabsorbent composite (s) based on dialdehyde cellulose extracted from banana fiber waste. Carbohydr Polym 343:122504
45. Bangar SP, Whiteside WS, Kajla P, Tavassoli M (2023) Value addition of rice straw cellulose fibers as a reinforcer in packaging applications. Int J Biol Macromol 243:125320
46. He X, Jiang J, Hong Z, Pan X, Dong Y, Xu R (2020) Effect of aluminum modification of rice straw–based biochar on arsenate adsorption. J Soils Sediments 20:3073–3082
47. Mioč U, Mojović Z, Jovanović DM (2016) Multielectron Redox Catalysts. Encycl Membr 1346–1348
48. Faulkner JS, Stocks GM, Wang Y (2018) Multiple Scattering Theory: Electronic Structure of Solids. IOP Publishing
49. Atli A, Noyel J-P, Hajjar A, Antouly K, Lemaire E, Simon S (2022) Exploring the mechanical performance of BaTiO3 filled HDPE nanocomposites: A comparative study of the experimental and numerical approaches. Polymer (Guildf) 254:125063
50. Shagali AA, Hu S, Li H, Chi H, Qing H, Xu J, Jiang L, Wang Y, Su S, Xiang J (2023) Thermal behavior, synergistic effect and thermodynamic parameter evaluations of biomass/plastics co–pyrolysis in a concentrating photothermal TGA. Fuel 331:125724
51. Budrugeac P (2010) Theory and practice in the thermoanalytical kinetics of complex processes: Application for the isothermal and non-isothermal thermal degradation of HDPE. Thermochim Acta 500:30–37
52. Mathew AP, Chakraborty A, Oksman K, Sain M (2006) The structure and mechanical properties of cellulose nanocomposites prepared by twin screw extrusion. ACS Publications
53. Mathew AP, Oksman K, Sain M (2005) Mechanical properties of biodegradable composites from poly lactic acid (PLA) and microcrystalline cellulose (MCC). J Appl Polym Sci 97:2014–2025
54. Petersson L, Oksman K (2006) Preparation and properties of biopolymer-based nanocomposite films using microcrystalline cellulose. ACS Publications
55. Bondeson D, Oksman K (2007) Dispersion and characteristics of surfactant modified cellulose whiskers nanocomposites. Compos Interfaces 14:617–630
56. Reis JML, Pacheco LJ, da Costa Mattos HS (2013) Tensile behavior of post-consumer recycled high-density polyethylene

at different strain rates. Polym Test 32:338–342
57. Henriksson M, Berglund LA, Isaksson P, Lindström T, Nishino T (2008) Cellulose nanopaper structures of high toughness. Biomacromolecules 9:1579–1585
58. Spencer MW, Cui L, Yoo Y, Paul DR (2010) Morphology and properties of nanocomposites based on HDPE/HDPE-g-MA blends. Polymer (Guildf) 51:1056–1070
59. Nie X, Xie Y, Ding X, Dai L, Gao F, Song W, Li X, Liu P, Tan Z, Shi H (2024) Highly elastic, fatigue-resistant, antibacterial, conductive, and nanocellulose-enhanced hydrogels with selenium nanoparticles loading as strain sensors. Carbohydr Polym 334:122068
60. Chen, Y., & Zhang L (2022) Enhancing the mechanical properties of polymers through nanofiller reinforcement. JMaterials Sci Eng R Reports 144:. https://doi.org/10.33887/rjpbcs/2019.10
61. Callister Jr WD, Rethwisch DG (2020) Materials science and engineering: an introduction. John wiley & sons
62. Nair LS, Laurencin CT (2007) Biodegradable polymers as biomaterials. Prog Polym Sci 32:762–798
63. Dai M, Zhao F, Fan J, Li Q, Yang Y, Fan Z, Ling S, Yu H, Liu S, Li J (2022) A Nanostructured Moisture-Absorbing Gel for Fast and Large-Scale Passive Dehumidification. Adv Mater 34:2200865
64. Petersson L, Oksman K (2006) Biopolymer based nanocomposites: comparing layered silicates and microcrystalline cellulose as nanoreinforcement. Compos Sci Technol 66:2187–2196